HREM: a Useful Tool to Formulate New Members of the Wide Bi^{3+}/M^{2+} Oxide Phosphate Series

Marielle Huvé,* Marie Colmont, and Olivier Mentré

Laboratoire de Cristallochimie et Physicochimie du Solide, CNRS UMR 8012, ENSCL, USTL, BP.108, F-59652 Villeneuve d'Ascq Cedex, France

Received February 6, 2004

A number of double Bi^{3+}/M^{2+} oxide phosphates have been isolated and structurally described using variable arrangements of isolated $[Bi-M-O]^{n+}$ polycations surrounded by PO_4 groups. The relationship between them leads to suspecting a great number of new arrangements within new compounds. In this work, the use of electron diffraction associated with high resolution imaging has considerably facilitated the prospecting. On the basis of the strong contrast observed by HREM between polycations of variable width and the interspace, a high-resolution image code and formulation rules have been established. This has allowed the formulation of original compounds, first detected in multiphased samples, yielding the synthesis of single-phased materials essential for the structural and physical characterization. This paper illustrates the complementarity between X-ray diffraction and electron microscopy studies to be especially well suited in this family of materials.

Introduction

Several double Bi^{3+}/M^{2+} related oxide phosphates have been isolated including the reported BiM_2XO_6[1−9] (M = Mg, Ca, Cu, Cd, Pb, and X = P, V, As) ($a \approx 11.5$, $b \approx 5.2$, and $c \approx 7.8$ Å), $Bi_{\sim 1.2}M_{\sim 1.2}PO_{5.5}$[10] (M = Mn, Co, Zn) ($a \approx 11.3$, $b \approx 5.4$, and $c \approx 15$ Å), $Bi_{\sim 6.2}Cu_{\sim 6.2}P_5O_{28}$[11] ($a \approx 11.6$, $b \approx 5.2$, and $c \approx 37.5$ Å).

The family connections between the several materials have first been suggested because of two common parameters (conventionally *a* and *b*) of their orthorhombic unit cell. In a second stage, common structural entities have been evidenced leading to strong topological relationships which reinforce the family appellation. As detailed in a previous work, an original descriptive concept recently developed for BiM_2XO_6 and $Bi_{\sim 1.2}M_{\sim 1.2}PO_{5.5}$ compounds[12] has been used instead of a classical description based on the association of oxygenated polyhedra. Effectively, it appears that, because of mixed aliovalent crystallographic Bi^{3+}/M^{2+} sites, the anionic polyhedra are strongly disordered in most cases. The mineral framework was consequently considered as an assembly, by shared edges, of $O(Bi,M)_4$ polyhedra in infinite ribbons of variable width: one, two, three, ... tetrahedra wide, surrounded by more or less disordered PO_4 groups. The obtained ribbons' structure and arrangement are responsible for two common lattice parameters. It is noteworthy that infinite $[Bi_2O_2]^{2+}$ layers corresponding to the 2D extension of our ribbon models are found in the Aurivillius series.[13−14]

The relationship between the already established crystal structures leads to suspecting a great number of new oxide phosphates, while prospecting is considerably facilitated by the use of electron diffraction associated with high-resolution (HR) imaging. As a matter of fact, the first advantage of these techniques applied to our materials is to explore crystallites of a powder one by one; which is very informative in the case of multiphased samples. At this point, it is helpful to point out that, as a direct consequence of both Bi^{3+}/M^{2+} occupancy (yielding narrow solid solution domains) and the number of antagonist family members, single-phased samples formulation and synthesis are very delicate. As a matter of fact, the different possible materials are gathered in a small area of the $Bi_2O_3-P_2O_5-MO$ diagrams. In addition, electron diffraction leads to the unambiguous determination of the lattice parameters (not favored by large unit cells showing pseudo symmetries between heavy Bi−O−M ribbons) as well as the evidence of the existence of hellicoidal axe and by comparison of the

* To whom correspondence should be addressed. Tel.: +33-320-337-721. Fax: +33-320-436-814. E-mail: huve@ensc-lille.fr.

(1) Huang, J.; Gu, Q.; Sleight, A. W. *J. Solid State Chem*. **1993**, *105*, 599.
(2) Abraham, F.; Ketatni, M.; Mairesse, G.; Mernari, B. *Eur. J. Solid State Chem*. **1994**, *31*, 313.
(3) Tancret, N. PhD Dissertation, Université des Sciences et Technologies de Lille: France, 1995.
(4) Mizrahi, A.; Wignacourt, J. P.; Steinfink, H. *J. Solid State Chem*. **1997**, *133*, 516.
(5) Mizrahi, A.; Wignacourt, J. P.; Drache, M.; Conflant, P. *J. Mater. Chem*. **1995**, *5*, 901.
(6) Ketatni, M.; Mernari, B.; Abraham, F.; Mentre, O. *J. Solid State Chem*. **2000**, *153*, 48.
(7) Giraud, S.; Mizrahi, A.; Drache, M.; Conflant, P.; Wignacourt, J. P.; Steinfink, H. *Solid State Sci.* **2001**, *3*, 593.
(8) Abraham, F.; Ketatni, M.;.Mernari, B. *Adv. Mater. Res.h* **1994**, *1*, 2.
(9) Xun, X.; Uma, S.; Sleight, A. W. *J. Solid State Chem*. **2002**, *167*, 245−248.
(10) Abraham, F.; Cousin, O.; Mentre, O.; Ketatni, M. *J. Solid State Chem*. **2002**, *167*, 168.
(11) Ketatni, M.; Huve, M.; Abraham, F.; Mentre, O. *J. Solid State Chem*. **2002**, *172* (*2*), 327.
(12) Colmont, M.; Huvé, M.; Ketatni, M.; Abraham, F.; Mentré, O. *J. Solid State Chem*. **2003**, *176* (*1*), 221.
(13) Vannier, R. N.; Mairesse, G.; Abraham, F.; Nowogrocki, G. *J. Solid State Chem*. **1996**, *122*, 394.
(14) Butterey, D. J.; Vogt, T.; Yap, G. P. A.; Rheingold, A. L. *Mater. Res. Bull.* **1997**, *32*, 947.

10.1021/cm040152j CCC: $27.50
Published on Web 06/05/2004

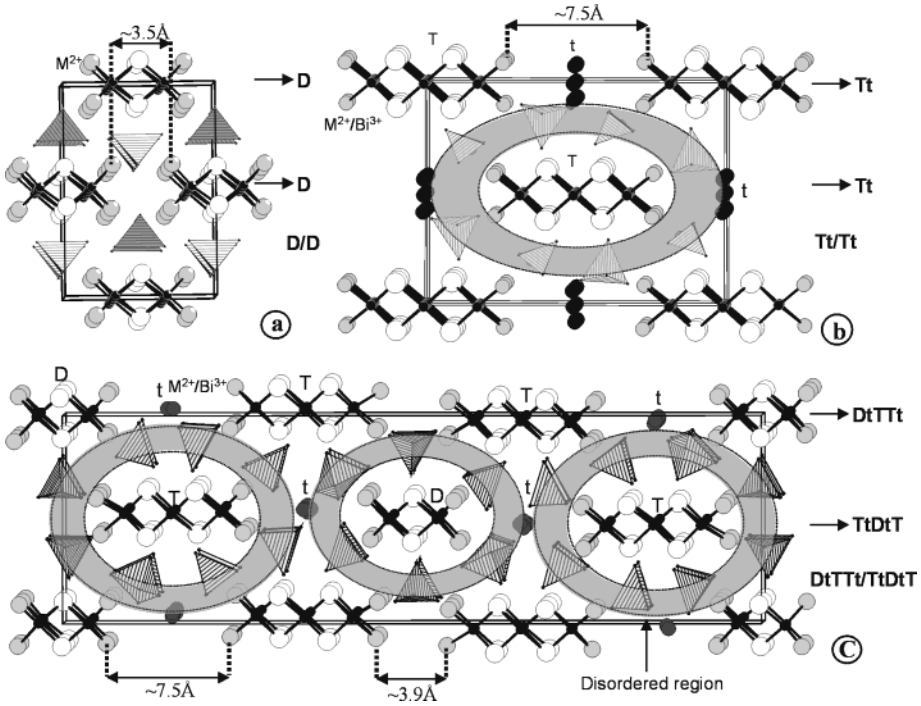

Figure 1. Projection on (0 1 0) of the structures of ribbon-possessing compounds, showing the T, D, t nomenclature: (a) BiM_2PO_6; (b) $Bi_{\sim 1.2}M_{\sim 1.2}(PO_4)O_{1.5}$; (c) $Bi_{\sim 6.2}Cu_{\sim 6.2}(PO_4)_5O_8$. The gray rings represent the disordered space existing because of the mixed nature of edges of ribbons sites (gray atoms).

zero order Laue zone (ZOLZ) and first-order Laue zone (FOLZ) the Bravais lattice and the glide planes present[15] (not easy by means of XRD data for disordered/defected single crystals). Furthermore, the superstructure phenomena, if they exist, are highlighted. The HR images show, on one hand, the structure projection which can be interpreted by means of image simulations, and, on the other hand, when possible, the structural origin of superstructure phenomena and defects.

The main purpose of this study is to formulate, from their HR images, new oxide phosphates of the reported family yielding the synthesis of pure sample essential for X-ray structural characterization. The analysis of the electron diffraction pattern (EDP) will be used to decide the real space group of the target crystallite, which will be helpful for the further structural refinement complicated by disorder effects. After a brief structural recall, the establishment of an image interpretation code from the HR images is reported for well-known structures. Such code has been used to interpret HR images of each of the new members found in this family from various chemical preparations.

Experimental Section

The different $Bi_wM_xO_y(XO_4)_z$ oxides (M = Mg, Ca, Cu, Cd, Pb, and X = P, V, As) reported in this work have been prepared from stoichiometric mixtures of Bi_2O_3, CdO, MO, and $(NH_4)_2HPO_4$. To avoid the problem of volatile species removal which implies several heating−grinding steps reaction from 200 to 800 °C for phosphate synthesis, the reactants have been dissolved in nitric acid and homogenized by stirring. A small amount of citric acid was added to complex and disperse the cations in the solution. The solution was then heated at 150 °C up to complete evaporation. The resulting powder was then dried, transferred to an alumina crucible, and heated at 5 °C/h to 800 °C for 48 h and quenched to room temperature. The purity of the samples has been checked by powder X-ray diffraction with a Siemens D-5000 diffractometer equipped with a graphite crystal diffracted-beam monochromator and Cu Kα radiation.

Electron diffraction patterns (EDP) were obtained on a JEOL 200CX, and high-resolution images were obtained on a JEOL 4000EX transmission electron microscope with a point resolution of 1.7 Å. In each case, the materials were crushed and dispersed on a holey carbon film deposited on a Cu grid. The computer-simulated HREM images were calculated using the JEMS program.[16]

Structural Recall

It is necessary to recall the structure of the parent compounds BiM_2XO_6,[1−9] $Bi_{\sim 1.2}M_{\sim 1.2}PO_{5.5}$,[10] and $Bi_{\sim 6.2}Cu_{\sim 6.2}P_5O_{28}$[11] previously studied by single-crystal X-ray diffraction.

A nomenclature based on T, D, and t sequence previously described in ref 12 is useful. In this notation, D and T refer respectively to 2- (double) and 3- (triple) tetrahedra-wide polycationic ribbons, while t represents M^{2+} tunnels sometimes formed by surrounding PO_4 between two subsequent ribbons. The nomenclature consists of using the appropriate TDt sequence along the *c* axis centered at $x = 0$ and $x = 1/2$ separated by a slash (/) as detailed below.

BiM_2XO_6 crystal structure ($a \approx 11.5$, $b \approx 5.2$, $c \approx 7.8$ Å) consists of two rows of double ribbons centered at $x = 0$ and $1/2$ involving a D/D sequence (Figure 1a). It exhibits two-tetrahedra-wide ribbons surrounded by six phosphate groups PO_4^{3-}. This general scheme is always valid, even if the tilt of the PO_4 can induce different space groups depending on the M and X nature.[6] The *b*

(15) Morniroli, J. P.; Steeds, J. W. *Ultramicroscopy* **1992**, *45*, 219−239.

(16) JEMS. Electron microscope software. Copyright P. STADELMANN 1999−2004 CIME EPFL, Switzerland.

unit cell parameter ~5.2 Å is twice the height of one $O(Bi,M)_4$ tetrahedron. Within the double ribbons, Bi^{3+} solely occupies the central positions and M^{2+} occupies the edges, leading to a well-ordered stoichiometric compound. The 3.5-Å-wide space existing between double ribbons along *c* is too narrow to incorporate M^{2+} hosts. No t tunnel exists in the BiM_2XO_6 framework.

$Bi_{\sim 1.2}M_{\sim 1.2}PO_{5.5}$ ($a \approx 11.3$, $b \approx 5.4$, $c \approx 15$ Å) shows triple ribbons separated by tunnels at $x = 0$ and $^1/_2$, i.e., a Tt/Tt sequence (Figure 1b). Each ribbon is surrounded by eight phosphate groups. The centers of the ribbons are solely occupied by Bi^{3+} while the edges are mixed Bi^{3+}/M^{2+} positions. The tunnels, located between two triple ribbons along *c*, are partially occupied by M^{2+} (the distance of 7.5 Å between two triple chains along *c* is considerably longer than that for the previous compound, which allows the creation of tunnels between two neighboring T). These disordered features lead to possible deviation from both a strict formula and a strict symmetry for Tt/Tt compounds. Therefore, the *Icma* space group has been validated for M = Co^{2+} and Mn^{2+}.[10]

$Bi_{\sim 6.2}Cu_{\sim 6.2}P_5O_{28}$ ($a \approx 11.6$, $b \approx 5.2$, $c \approx 37.5$ Å) shows the complex DtTTt/TtDtT sequence (Figure 1c) and could be considered as an intergrowth of the two previously reported structures. The previous remarks concerning Bi and Bi/M locations in the center and the edges of the ribbons still hold. In this structure, tunnels occupied by M^{2+} are located between one triple- and one double-ribbon which are separated by 7.5 Å along *c*. The distance between two T ribbons along *c* is too short (≈3.9 Å) to accommodate M^{2+} cations. Several compositions show evidence of this crystal structure but the space group assigned to the above formula single crystals is $Pn2_1a$.

The structural relationship between these three oxide phosphates is based on polycationic ribbons arrangements. Their structure results in D and T ribbons surrounded by PO_4^{3-} groups forming, when possible, t tunnels containing M^{2+}.

The organization of ribbons is responsible for the two common parameters *a* and *b*, as follows. The *b* parameter (≈5.2−5.4 Å) is characteristic of the infinite ribbons' axes and corresponds to the height of two edge-sharing tetrahedra. The *a* parameter (≈11.5−12 Å) is twice the distance between the sheets of ribbons isolated by PO_4 rows. The *c* parameter depends on the width and arrangement of the ribbons.

It is interesting to summarize, in view of further new formulation, some structural features which can be called "formulation rules" deduced from structural observations of the parent compounds.[11] (a) D, ~ 5 Å long, and T, ~ 8 Å long, are surrounded by six and eight phosphate groups, respectively, leading to a quantifiable PO_4/ribbon ratio. (b) Within the ribbons, the central tetrahedra atoms are necessarily OBi_4. The borders host mixed Bi^{3+}/M^{2+} crystallographic positions. (c) The t tunnels partially occupied by M^{2+} hosts are created at the center of surrounding PO_4 if the distance between ribbons (along *c*) is close to 7 Å. For values around 4 Å the space is too small to receive cations. (d) The tunnels formed by phosphate groups can be occupied by M^{2+} atoms in a very disordered manner and are not necessarily fully occupied.

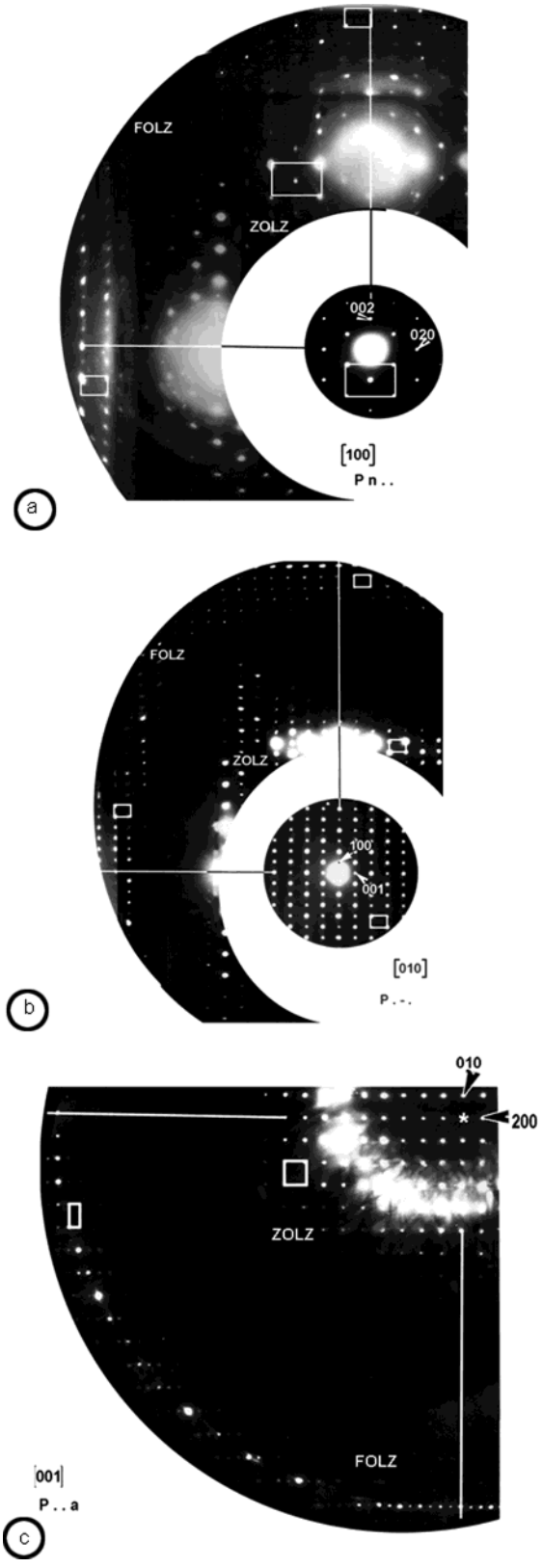

Figure 2. D/D sequence ($BiCu_2PO_6$ sample). Zone axis pattern of the basic zones. (a) [100], (b) [010], (c) [001], leading to the extinction symbol Pn-a (- means no glide plane).

Image Interpretation Code. This code is dedicated to the determination of structural features from HR images, i.e., wideness and sequence of the ribbons, and existence or nonexistence of tunnels between them. This has been established with the help of image simulations

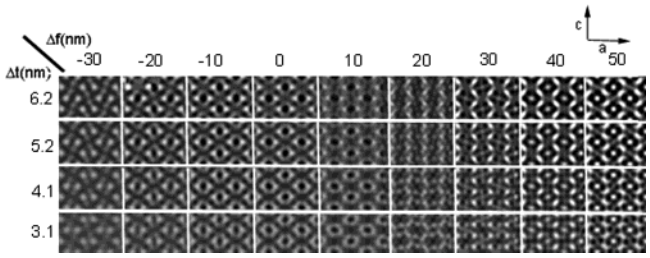

Figure 3. D/D sequence ($BiCu_2PO_6$ sample). [010] high-resolution image: images have been simulated on the basis of X-ray structure data for various values of defocus and thickness.

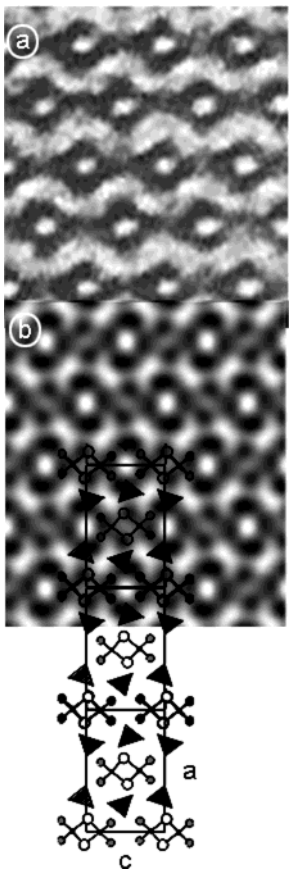

Figure 4. D/D sequence ($BiCu_2PO_6$ sample). [010] high-resolution images: (a) experimental image, (b) simulated image for a defocus of 50 nm and a thickness of 4.1 nm. A superposition of the structure projection on the images allows direct interpretation of the contrast.

based on the X-ray structure refinement of the three previous compounds. Considering, by convention, the axis ~5.4 Å as the *b* axis, the most relevant zone axis is [010] because it shows images perpendicular to the infinite ribbons' axis and displays the arrangement of ribbons.

D/D Sequence ($BiCu_2PO_6$ Sample). *Electron Diffraction*. The comparison (Figure 2) between the periodicity and the shifting of the ZOLZ and the first-order Laue zone (FOLZ) leads to the extinction symbol Pn-a (- means no glide plane),[13] which is in accordance with the *Pnma* space group used for the structural refinement.

[010] High-Resolution Image. First, images have been simulated on the basis of the X-ray structure data for various values of defocus and thickness (Figure 3). One experimental image (Figure 4) has been satisfactorily

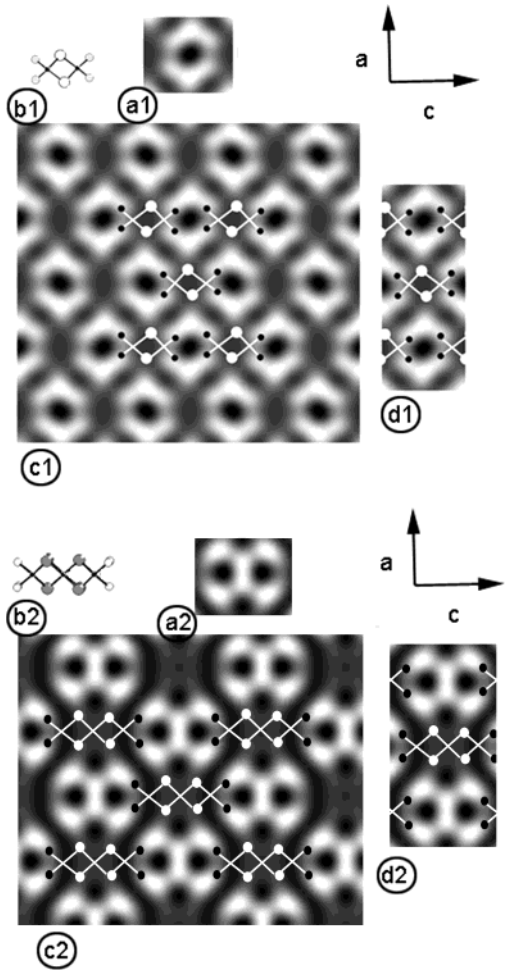

Figure 5. Image code. Top D/D sequence: (c1) simulated image (defocus = −10 nm, thickness = 4.1 nm) from the series of Figure 3. White circles (a1) are closely related to the presence in the structure of (b1) double chains (D). (c1) The superposition of the projected ribbons (along b) shows (d1) that double chains are located between two white circles along a and c. Bottom Tt/Tt sequence: (c2) simulated image (defocus = −10 nm, thickness = 4.3 nm) from the series of Figure 8. White crosses (a2) are closely related to the presence in the structure of (b2) triple chains (T). (c2) the superposition of the projected ribbons (along b) shows (d2) that triple chains are located between two white crosses along a and c.

simulated for a defocus of 50 nm and a thickness of 4.1 nm, which proves the validity of the structure and authenticates the series of image simulation. The contrast is characterized by white zigzag (Figure 4a) assigned, according to the image simulation, to PO_4^{3-} phosphate groups. In the series of image simulations (Figure 3), the zigzag progressively transforms into white circles based contrasts, for a defocus of −10 nm and a thickness of 4.1 nm, which will be part of the interpretation code. We had special interest in the (a,c) plane which contains the DTt sequence information (along c) and ribbons/PO_4 stacking (along a). The images are characterized by white circles (Figure 5a1) which are formed by 4 edges of ribbons and 2 PO_4 (Figure 5b1). As a matter of fact, the superposition of the projected ribbons (Figure 5c1) shows that double chains are located between two white circles along a (Figure 5d1). Therefore, the presence of white circles in the image contrast should be an indication of the presence of double chains and a first block of the image code.

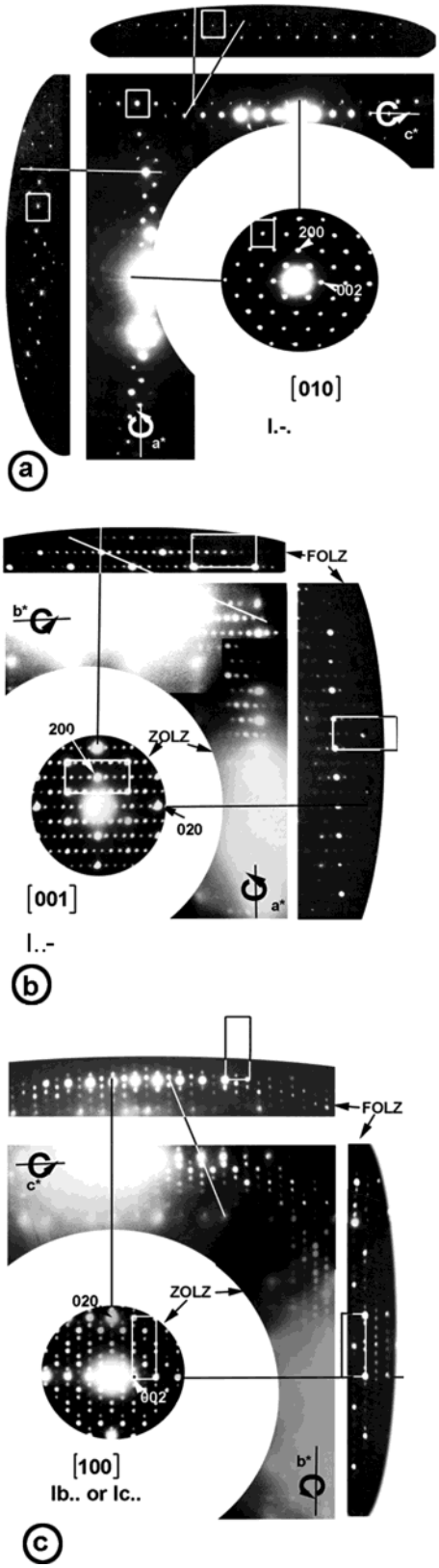

Figure 6. Tt/Tt sequence ($Bi_{1.2}Co_{1.2}PO_{5.5}$ sample). Basis zone axis patterns: (a) [010], (b) [001], (c) [100]. The main spots corresponding to the cell refined from X-ray diffraction data are indexed. Additional modulation spots are observed in the (b) [001] and (c) [100] ZAP. The extinction symbol for intense spots is Ic- -.

Tt/Tt Sequence ($Bi_{1.2}Co_{1.2}PO_{5.5}$ Sample). *Electron Diffraction*. The basic zone axis patterns (ZAP) are shown in Figure 6. The main spots corresponding to the

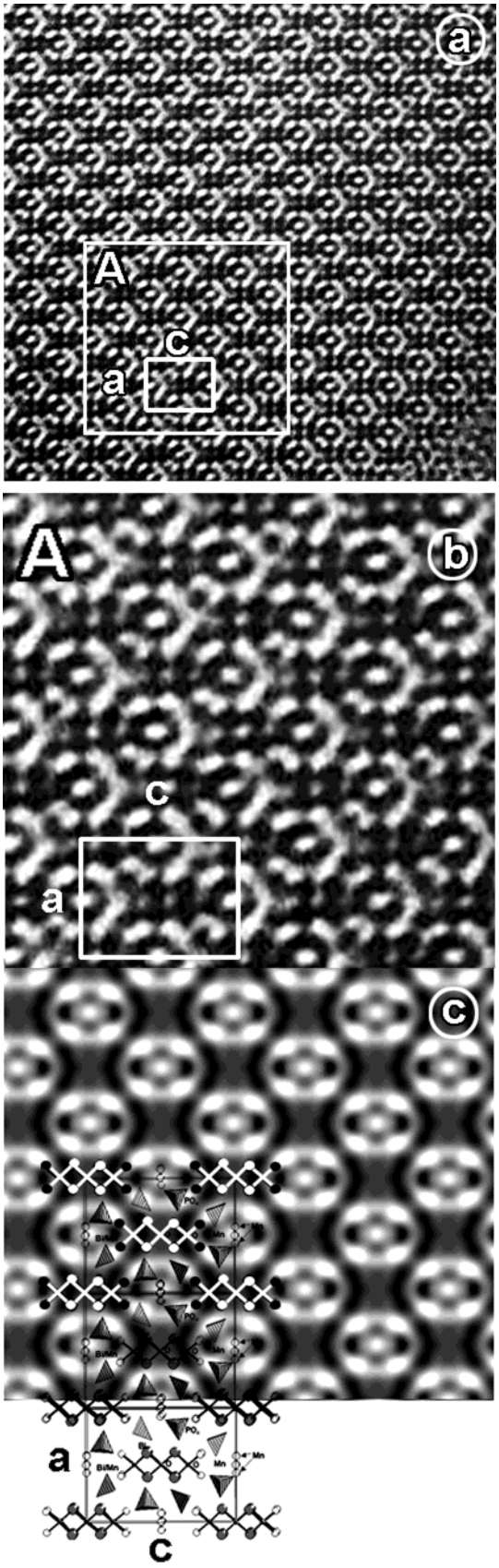

Figure 7. Tt/Tt sequence ($Bi_{1.2}Co_{1.2}PO_{5.5}$ sample). (a) [010] experimental high-resolution image and (b) enlargement of the zone A. (c) simulated image for a defocus of 20 nm and a thickness of 4.3 nm: white centered blocks can be attributed to PO_4^{3-} (perimeter of the circle) and Co tunnel position (t) (central white dot) according to the structure projection.

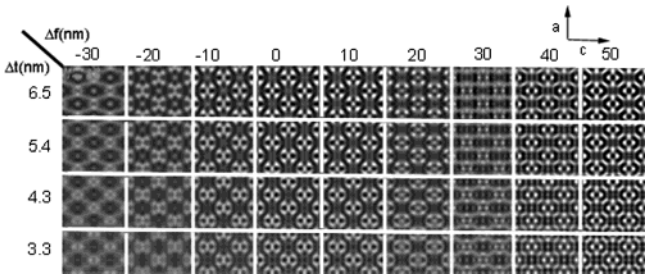

Figure 8. Tt/Tt sequence ($Bi_{1.2}Co_{1.2}PO_{5.5}$ sample). [010] through-focus series calculated on the basis of the X-ray structure refinement results.

cell refined from X-ray diffraction data are indexed, but additional modulation spots related to incommensurate phenomena are observed in the [001] and [100] ZAP. They are not the subject of this paper and will be carefully studied in another work. Only the intense spots (indexed in Figure 6) are considered here. The extinction symbol for basic spots is Ic- -, which is not really in accordance with the *Icma* space group used for the structural refinement of $Bi_{\sim 1.2}M_{\sim 1.2}PO_{5.5}$ (M = Co, Mn)[10](performed before the ED study). This suggests extra phenomena at the microscopic crystallite scale largely lost at the single-crystal scale which may be due to the ordering of Bi/M edges of ribbons.

[010] High-Resolution Image. Experimental images (Figure 7) show the perfect periodicity in this projection for a defocus of 20 nm and a thickness of 4.3 nm. The contrast is constituted by white-centered circles that correspond to a perimeter made of 4 PO_4^{3-} positions and 4 edges of ribbons centered around the Co-tunnel positions (t) (central white dot). A through focus series was calculated on the basis of the X-ray structure refinement results and shows the progressive change of the circles into white cross-like shapes for a −10-nm defocus and a thickness of 4.3 nm (Figure 8). Then, for this simulation, as observed in Figure 5a-d2, T chains are placed in the dark contrast between two subsequent white crosses along a. The contrast image interpretation code is now established to identify D and T ribbons. White circles (Figure 5_1) and white crosses (Figure 5_2) in an image are directly correlated to respectively D and T chains. The code will be applied to a mixed T/D material in the next section.

DtTTt/TtDtT Sequence ($Bi_{6.2}Cu_{6.2}P_5O_{28}$ Sample). *Electron Diffraction.* As in the previous case, superstructure phenomena appear in the EDP (white and black arrows (in Figure 9a and b), and black arrows indicate a supplementary LZ (in Figure 9c) but are not considered here. The main spots are indexed in the basic cell refined from X-ray data. The partial extinction symbol Pn-a is in accordance with the *Pnma* space group of the structure refined for a $Bi_{\sim 6.2}Cu_{\sim 6.2}P_5O_{28}$ single crystal.

[010] High-Resolution Image. Experimental image is shown in Figure 10a1. The contrast is formed by white circles and crosses similar to the contrasts of the image code. To check the validity of the image code, we first tried to locate the ribbons from the observed contrast without any structural help. It has been established that D chains lie between two circles along a (Figure 10a2) while T ribbons lie between two crosses along a (Figure 10a3). This code applied to the experimental image

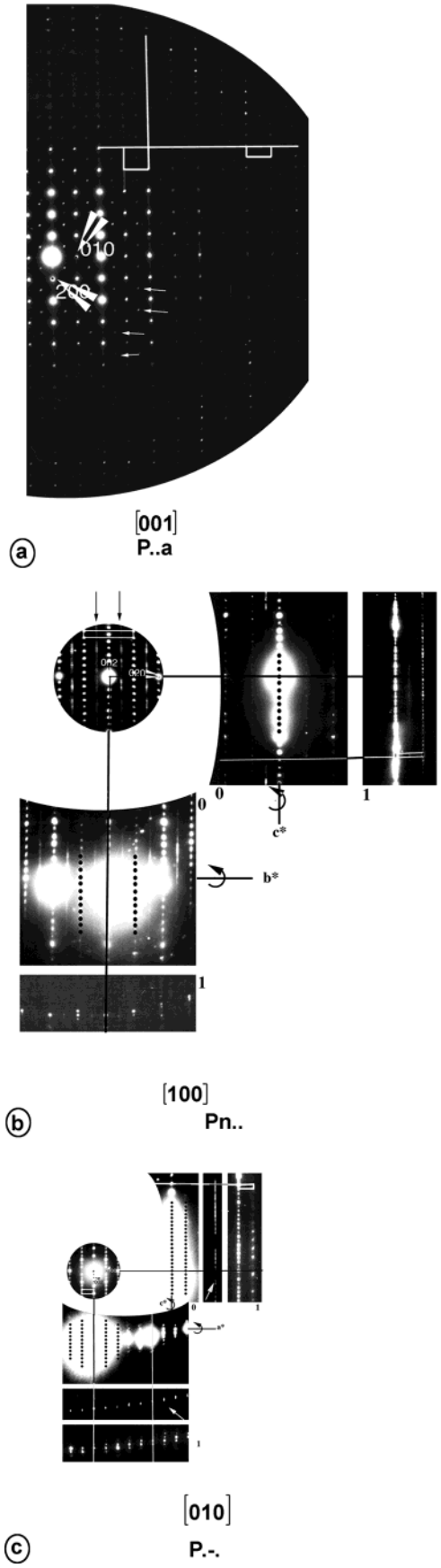

Figure 9. DtTTt/TtDtT sequence ($Bi_{6.2}Cu_{6.2}P_5O_{28}$ sample). Basis zone-axis patterns. (a) [001], (b) [100], (c) [010]. Superstructure phenomenon appears in the EDP (a,b) (white and black arrows) and (c) black arrows indicate a supplementary LZ. The partial extinction symbol (for intense spots) is Pn-a.

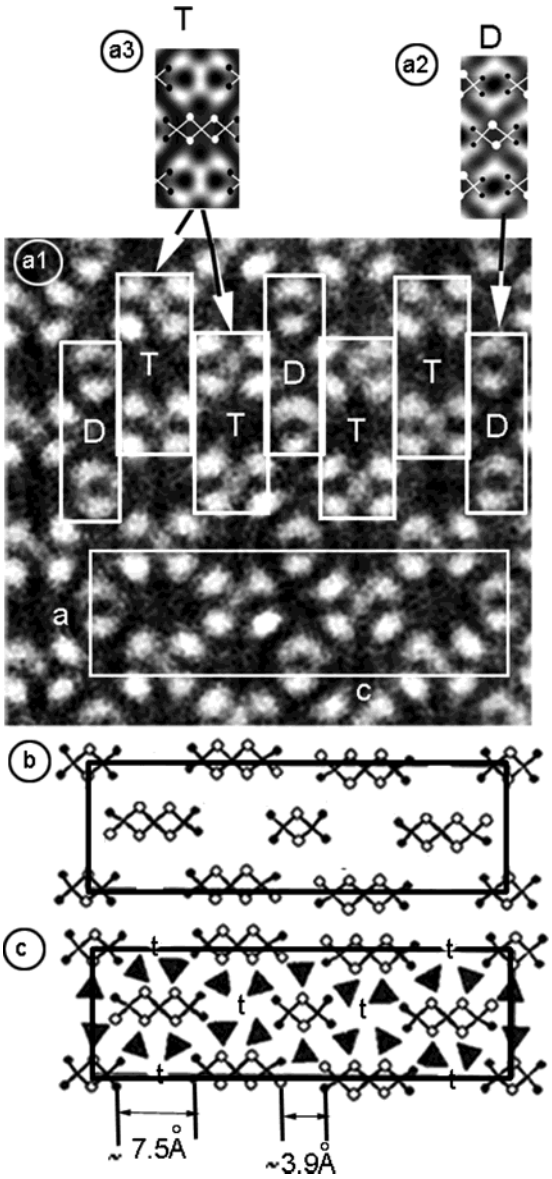

Figure 10. DtTTt/TtDtT sequence ($Bi_{6.2}Cu_{6.2}P_5O_{28}$ sample). [010] high resolution image: (a1) experimental image. Considering the image interpretation code (Figure 5), that is (a2) between two circles along a we find D chains, while (a3) T ribbons lie between two crosses. (b) the experimental image yields the DTT/TDT sequence; (c) the formulation rules enable approximately locating PO_4 groups and the tunnels t.

yields the DTT/TDT sequence represented in Figure 10b. The formulation rules previously established enable approximately locating PO_4 groups, because D (~5 Å long) and T (~8 Å long) are surrounded by, respectively, six and eight phosphate groups (Figure 10c). Even if the contribution of tunnels to the contrast is weak, they are easily located from steric considerations by analogy with the two previously investigated compounds. This leads to the DtTTt/TtDtT type, where "t" tunnels lie between triple and double ribbons separated by ~7 Å along c. As a matter of fact, the crosses are centered around "t" tunnels as previously observed.

Chemical Formulation. Taking into account the several rules announced above and the established model, it is easy to formulate possible materials from electroneutrality consideration. Thus, the investigated compounds can be formulated $D_2T_4t_4(PO_4)_{20}$ with D = $[Bi_2M_4O_4]$ and T = $[Bi_4M_4O_6]$, where Bi corresponds to the central bismuth-only sites and M stands for possible mixed Bi^{3+}/M^{2+} positions at the edges of ribbons. The tunnels are partially filled in order to balance the electroneutrality of the crystal for various Bi^{3+}/M^{2+} ratios. In this case, it appears that several compounds can be prepared pure, including the compound $Bi_{6.2}Cu_{6.2}P_5O_{28}$ that can be developed $[Bi_{2.4}Cu_{3.6}O_4]_2$ $[Bi_5Cu_3O_6]_4$ $Cu_{5.6}$ $(PO_4)_{20}$. The complete XRD (single crystal + powder) and HREM investigation is reported in ref 11 and verifies the deduced crystal structure sequence and possible formulation. Images have been calculated on the basis of the atomic positions given by the X-ray results for various defocus values and thicknesses (Figure 11). Experimental images match well the simulated image for a defocus of −10 nm and a thickness of 4.2 nm (Figure 12). The superposition of the atomic position projection in this plane confirms the framework previously established from HR images and validates the image interpretation code.

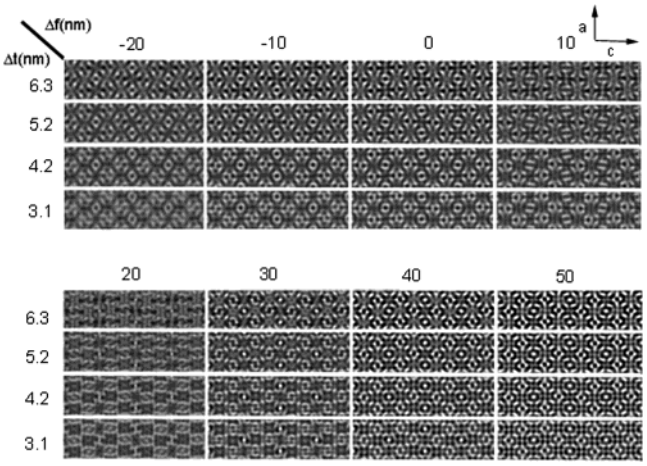

Figure 11. DtTTt/TtDtT sequence ($Bi_{6.2}Cu_{6.2}P_5O_{28}$ sample). Images calculated on the basis of the atomic positions given by the X-ray results, for various defocus and thickness.

Image Code. At this point, it seems useful to summarize our process. According to two known crystal structure types, the following image code has been established from D/D and Tt/Tt and verified on the DtTTt/TtDtT complex sequence in perfect adequacy with the structure refined from X-ray data: (a) D are localized in the dark region between two white circles along a (and c)(Figure 5a-d1). (b) T are situated in the dark region between two crosses along a (and c)(Figure 5a-d2). Because the chains appear as dark contrast it prevents any possibility to distinguish the Bi^{3+} between the M^{2+} cation at the border of them in case of ordering. (c) Chemical considerations yield to the formulation of possible single-phase materials.

Application to New Family Members. As we have already mentioned in another work[12] it is not rare that, during our synthesis, the attempts to prepare one structural type lead to another one or a mixture of several types. At this level the TEM technique is informative because it tests crystallite per crystallite and allows a perfect sorting of the different phases, even minor phases, without any further structural knowledge.

Two different preparations that correspond to the $Bi_{\sim 3}Cd_{\sim 3.72}Co_{\sim 1.28}O_5(PO_4)_3$ and $Bi_{5.88}Cd_{4.58}Cu_{1.82}(PO_4)_5O_{7.72}$ chemical compositions reveal crystals which, after the

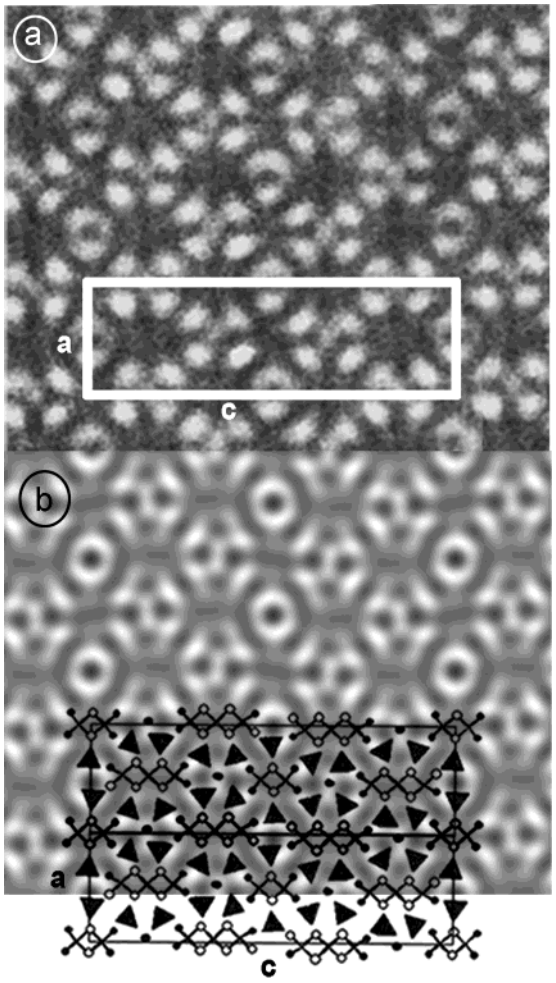

Figure 12. DtTTt/TtDtT sequence ($Bi_{6.2}Cu_{6.2}P_5O_{28}$ sample). (a) Experimental image matches well (b) simulated image for a defocus of −10 nm and a thickness of 4.2 nm. The superposition of the atomic position projection in this plane confirms the framework previously established from HR images and validates the image interpretation code.

reconstruction of the reciprocal space, exhibit parameters $a \approx 5$, $b \approx 11$, and $c \approx 23$ Å for the former and $c \approx 53$ Å for the latter. The *a* and *b* parameters indicate that there are probably new members of this family. But what about the structural polycationic sequence types of ribbons?

New TT/DtDt Sequence ($Bi_{\sim 3}Cd_{\sim 3.72}Co_{\sim 1.28}O_5(PO_4)_3$ Preparation). *Electron Diffraction*. Unit cell parameters $a \approx 11$, $b \approx 5$, and $c \approx 23$ Å. Obvious supplementary weaker spots are evidenced and will be studied in a further work. The partial extinction symbol for the basic intense spots is A b-- (- means no glide plan) (Figure 13).

[010] HR Image. It has been possible to obtain a HR image with white circles and crosses (Figure 14), that allows the application of the image code previously established. One can notice that a misleading $c \sim {}^{23}/_{2}$ Å is highlighted in the image: the observable periodicity in the [010] image is a halved image because of the A Bravais lattice.

From the established code, a TT/DD sequence represented in Figure 14b is deduced. Inter-ribbon width calculation yields the final TT/DtDt type with eight and six PO_4 tetrahedra around each T and D, respectively as shown in Figure 14c. The corresponding formula is

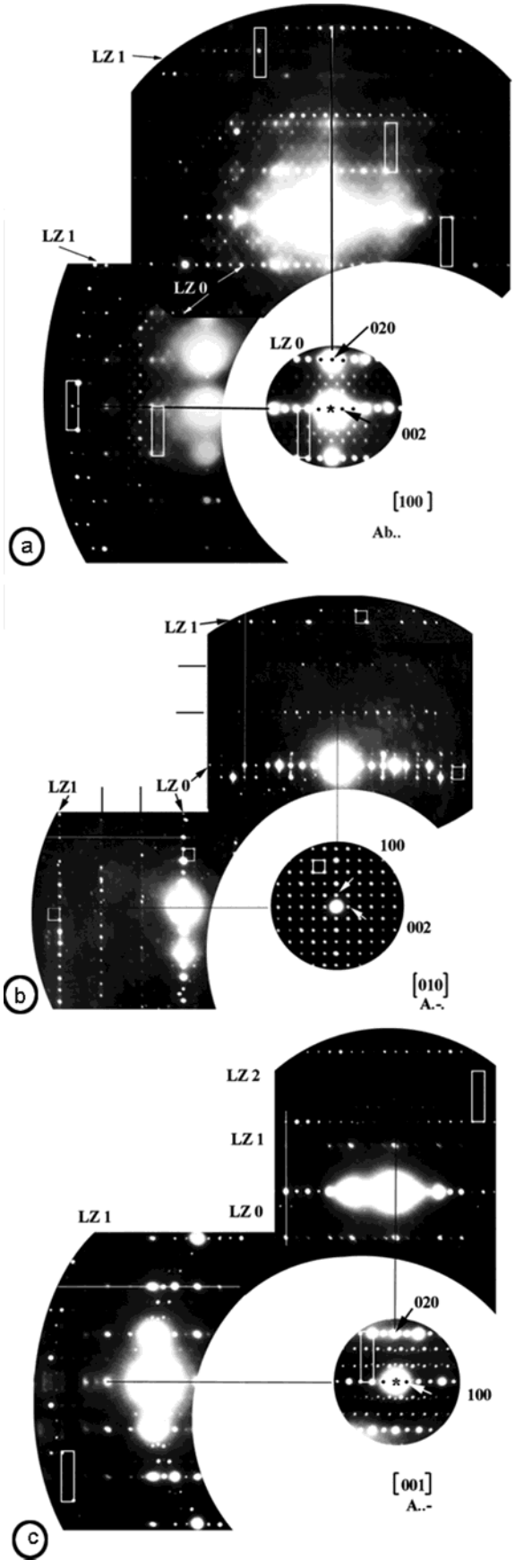

Figure 13. New TT/DtDt sequence ($Bi_{\sim 3}Cd_{\sim 3.72}Co_{\sim 1.28}O_5(PO_4)_3$ preparation). Basis zone−axis patterns: (a) [001], (b) [100], (c) [010]. Obvious supplementary weaker spots are evidenced. The partial extinction symbol for the basic intense spots is A b- - (- means no glide plan).

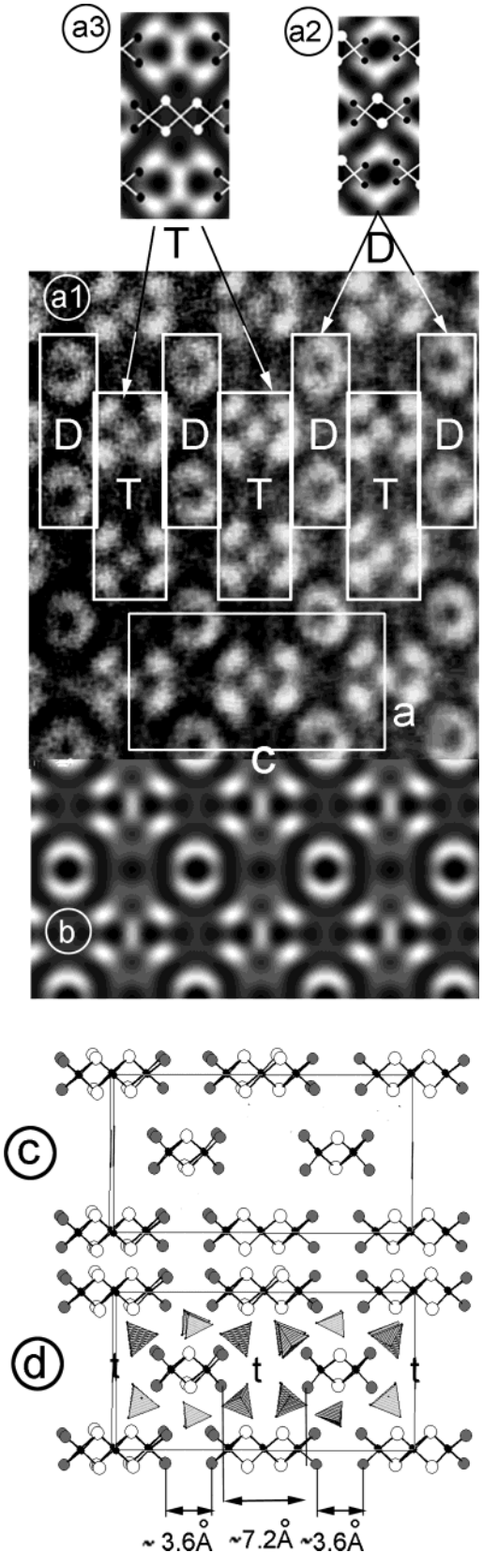

Figure 14. New TT/DtDt sequence ($Bi_{\sim 3}Cd_{\sim 3.72}Co_{\sim 1.28}O_5(PO_4)_3$ preparation). (a1) [010] experimental HR image. From the established code (a2) and (a3), a (c) TT/DD sequence is deduced. (d) Inter-ribbon width calculation yields the final TT/DtDt type with eight and six PO_4 tetrahedra around each T and D, respectively. (b) Image calculated on the basis of the atomic positions given by the X-ray results for a defocus of −10 nm and a thickness of 3.8 nm.

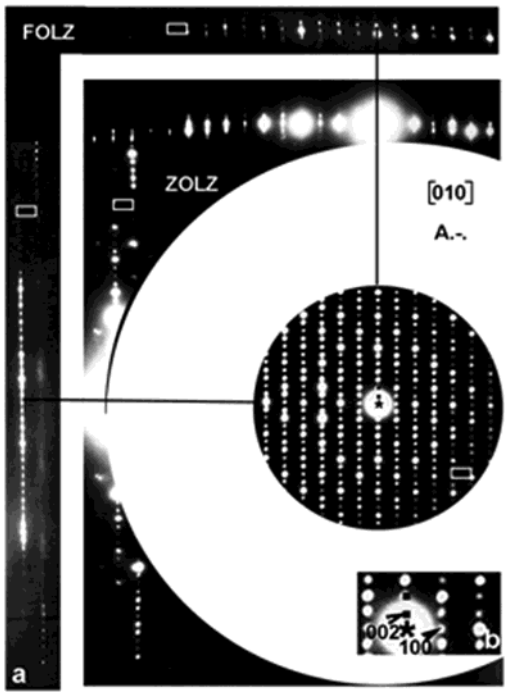

Figure 15. New TtDtTtDt/TTtTTt sequence ($Bi_{5.88}Cd_{4.58}Cu_{1.82}(PO_4)_5O_{7.72}$ preparation). [010] zone-axis patterns: (a) FOLZ and ZOLZ (b) enlargement of the ZOLZ. The partial extinction symbol for the basic intense spots is A.-. (- means no glide plan).

$T_2D_2t_2(PO_4)_{12}$ with D = $[Bi_2M_4O_4]$ and T = $[Bi_4M_4O_6]$, where Bi correspond to the central bismuth-only sites and M stand for possible mixed Bi^{3+}/M^{2+} positions at the edges of ribbons. The announced framework is a base but some incertitude related to Bi^{3+}/M^{2+} and M^{2+} tunnel occupancies stay to establish a precise composition. Furthermore, the problem is enlarged by the presence in the parent preparation of both Cd^{2+} and Co^{2+} for M^{2+} but, considering other works, we assume that Co^{2+} is a better candidate than Cd^{2+} in tunnels. Among a number of sample-preparation attempts, pure single-phased $Bi_3Cd_{3.72}Co_{1.28}O_5(PO_4)_3$ have been successfully prepared. The developed formula $[Bi_4Cd_4O_6]_2[Bi_2Cd_{3.44}Co_{0.56}O_4]_2Co_4(PO_4)_{12}$ was checked by single-crystal X-ray diffraction in the *Abmm* space group [12] and allows a simulation of image (Figure 14b) for a defocus of −10 nm and a thickness of 3.8 nm, which prove irrefutably the validity of the method used.

New TtDtTtDt/TTtTTt Sequence ($Bi_{5.88}Cd_{4.58}Cu_{1.82}(PO_4)_5O_{7.72}$ Preparation). *Electron Diffraction*. Unit cell parameters, $a \approx 11$, $b \approx 5$, and $c \approx 53$ Å. Once again, supplementary weaker spots are evidenced, but as it is not the purpose of this paper to consider them, we consider only the intense spots. It is necessary to admit that, because of the short c* parameter, it is difficult to obtain large magnification with, at the same time, the ZOLZ and FOLZ on the same [010] image and, therefore, it is not possible to determine with certitude the shift between the ZOLZ and FOLZ. Therefore, a partial extinction symbol for the basic intense spots is A.-., Figure 15. The part of the symbol which refers to the *a* and *c* axes cannot be surely determined because, on one hand, [001] ZAP cannot be identified certainly in a multiphase sample furthermore, because of the small value of c* the ZOLZ and FOLZ may overlap. On the

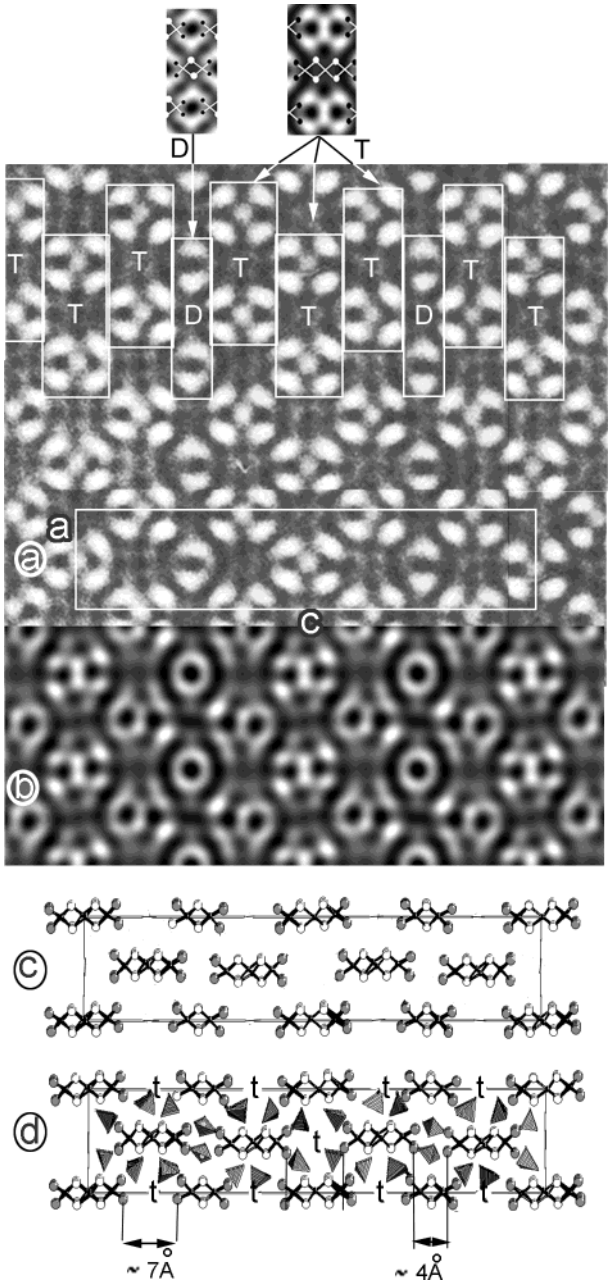

Figure 16. New TtDtTtDt/TTtTTt sequence ($Bi_{5.88}Cd_{4.58}Cu_{1.82}(PO_4)_5O_{7.72}$ preparation). (a) [010] experimental HR image: applying the image code to the image obtained allows (c) to localized the chains and their width. The sequence is TDTD/TTTT and (d) has been completed using phosphate environment rules of the chains and tunnels possible space calculations. This leads the TtDtTtDt/TTtTTt sequence. (b) Image calculated on the basis of the atomic positions given by the X-ray results for a defocus of −10 nm and a thickness of 4.3 nm.

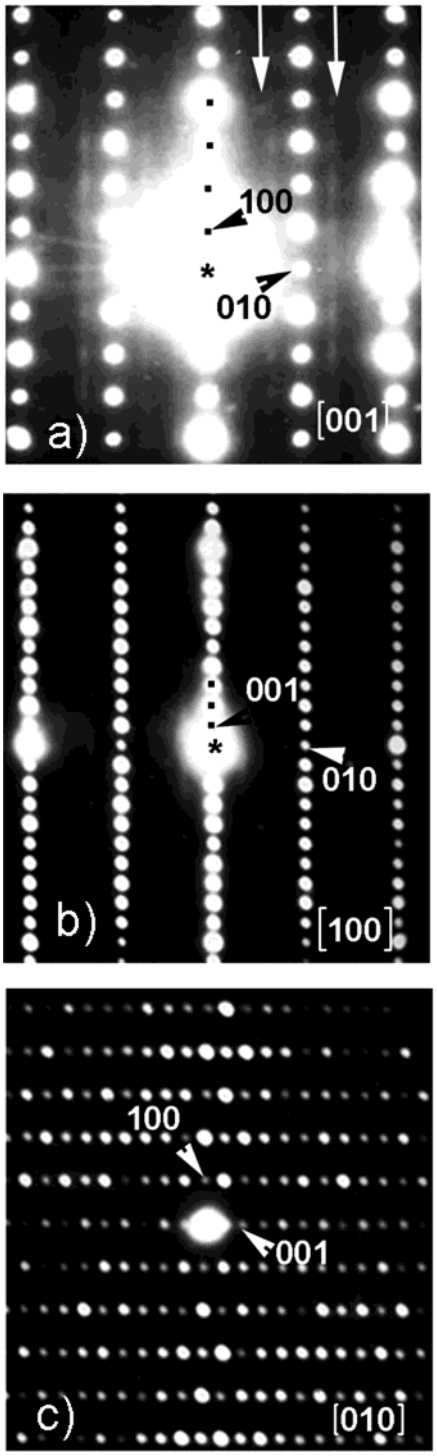

Figure 17. Other types of ribbons in new oxide phosphates. Basic patterns (a) [001], (b) [100], (c) [010]: according to the reconstitution of the reciprocal space, some crystals exhibit lattice parameters of $a \approx 11.5$, $b \approx 5.5$, $c \approx 25$ Å. Only weak strains are observed in the [001] EDP (white arrows) as supplementary phenomenon.

other hand, [100] ZAP's show satellite spots misleading the interpretation of intensity on crystal tilting.

[010] HR Image. Applying the image code to the image obtained (Figure 16a) allows localization of the chains and their width on Figure 16b. The sequence is TDTD/TTTT and has been completed using space calculations for tunnels. It leads the TtDtTtDt/TTtTTt sequence. In a second step, as previously managed, it is possible to approximately locate the phosphate groups (Figure 16c). The formula is $T_6D_2t_6(PO_4)_{28}$. Taking into account these previous considerations, pure single phase has been obtained for a composition of $Bi_{36}Cd_{24}Cu_8(PO_4)_{28}O_{44}$ and the X-ray study has been performed. The structure has been resolved in the *A*2/*m* (pseudo-orthorhombic) space group from single-crystal X-ray diffraction.[17] This small monoclinic distortion of the orthorhombic cell cannot be detected by means of electron diffraction. On the basis

(17) Colmont, M.; Huvé, M.; Mentré, O. **2004**, accepted for publication.

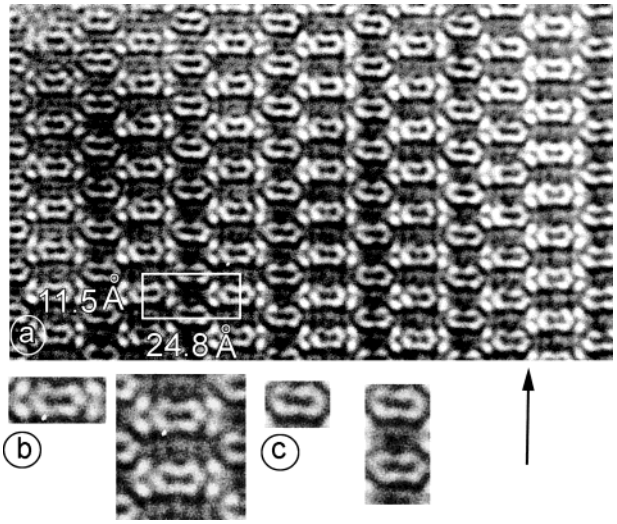

Figure 18. Other types of ribbons in new oxide phosphates. (a) *[010] Experimental HR Image*: (b) white ovals surrounded by four points which look like two extremities of arrows in opposite direction, and (c) white ovals are observed. A defect plane, identified as the lack of one extremity of arrow can be observed (black arrow).

of this structure data, image for a defocus of −10 nm and a thickness of 4.2 nm (Figure 16b) was calculated and represents an essential proof of the validity of the image interpretation code.

Other Types of Ribbons ($n > 3$) in New Oxide Phosphates. The HREM images observed for several other chemical preparations show different motifs and contrasts despite lattice parameters which suggest other members of this same family ($a \approx 11.5$, $b \approx 5.5$ Å). These materials are currently under investigation, but, at least, we can detail features observed on crystallites of the $Bi_{11}Co_{4.5}(PO_4)_6O_{12}$ sample which open a wide field of future experiments.

Electron Diffraction. Figure 17: according to the reconstitution of the reciprocal space, some crystals exhibit lattice parameters of $a \approx 11.5$ Å, $b \approx 5.5$, $c \approx 25$ Å. Only weak strains are observed in the [001] EDP (white arrows in Figure 17) as supplementary phenomenon.

[010] HR Image. Despite the values of common *a* and *b* parameters, the contrast of the HR image is different (Figure 18). White circles and crosses are not observed (or any other contrast of the through-focus series calculated for the compounds of the previous series, Figures 3, 7, and 11)), but white ovals surrounded by arrows headed in opposite direction (Figure 18b) and white ovals (Figure 18c) are observed. A defect plane, identified as the lack of one extremity of arrow can be observed (black arrows in Figure 18). This suggests that other combinations of ovals and arrows should be possible, yielding other structure configurations. At this stage of our study, it is possible to announce through single- crystal XRD data that the structure of the concerned ribbons is modified because of their expansion throughout $n > 3$ tetrahedra length, but as is usual in these materials, the cationic and PO_4 disorder avoid an easy crystal structure refinement. It is therefore viewable to interpret, as presented here, this new kind of HREM contrast through a new code to be established using the adapted parent compounds.

Conclusion

The formulation of an image code to interpret the HR images of the series of double Bi/M oxidephosphates has been very helpful to synthesize two new compounds. This code associated with chemical deductions has allowed accurate establishment of the structural framework consisting of the width and sequence of protagonist polycations as well as that of the location of the surrounding phosphate groups. But some incertitude concerning the formulation (nature of the border of ribbons and nature as well as the ratio of the ions in the t tunnel) exists and leads to a relative great number of composition tests to try to synthesize a single phase of the desired compound. Nevertheless we have succeed in preparing two new phases of this family, which allows a complete structural and physical investigation. Another kind of related oxide phosphate has been evidenced by different HREM image contrasts, in spite of lattice similarities. Therefore, a structural investigation by XRD is essential to determine structural characteristics of several terms of these "new" series, in order to establish the HR imaging code.

Acknowledgment. We thank Pr. F. Abraham (LCPS, University Lille, France) for help and discussion, the EMAT laboratory (Antwerp, Belgium) for microscopy facilities, and the Nord Pas de Calais region for financial support.

CM040152J